Impact of Bimolecular Recombination on the Fill Factor of A Fullerene and Non-Fullerene Based Solar Cell: A Comparative Study of Charge Generation and Extraction

Seyed Mehrdad Hosseini[1], Steffen Roland[1], Jona Kurpiers[1], Zhiming Chen[2], Kai Zhang[2], Fei Huang[2], Ardalan Armin[3], Dieter Neher[1], Safa Shoaee[1]*

[1]Institute of Physics and Astronomy, University of Potsdam, Karl-Liebknecht-Straße 24-25, D-14476 Potsdam-Golm, Germany

[2]Optoelectronics of Organic Semiconductors, Institute of Polymer Optoelectronic Materials and Devices, State Key Laboratory of Luminescent Materials and Devices, South China University of Technology, Guangzhou 510640, P. R. China

[3]Department of Physics, Swansea University, Singleton Park, Swansea SA2 8PP, Wales, UK

ABSTRACT. Power conversion efficiencies of donor:acceptor organic solar cells utilizing non-fullerene acceptors have now increased beyond the record of their fullerene-based counterparts. There remain many fundamental questions regarding nano-morphology, interfacial states, charge generation and extraction, and losses in these systems. Herein, we present a comparative study of

bulk heterojunction solar cells composed of a recently introduced nappthothiadiazole-based polymer (NT812) as the electron donor and two different acceptor molecules, namely PCBM[70] and ITIC. A comparison between the photovoltaic performance of these two types of solar cells reveals that the open circuit voltage (V_{oc}) of NT812:ITIC based solar cell is larger but the fill factor (FF) is lower than that of NT812:PCBM[70] device. We find the key reason behind this reduced FF in the ITIC-based device to be faster non-geminate recombination relative to the NT812:PCBM[70] system.

1. Introduction

Conventional organic solar cells (OSCs) consist of blends of electron donating materials and classical electron accepting fullerene-based molecules in the form bulk heterojunctions (BHJs). However, in the past few years, the focus in the development of OSCs has shifted to non-fullerene acceptors (NFAs); synthesizing and engineering systems with power conversion efficiencies (PCEs) of 13%.[1] While these materials achieve impressive short circuit current (J_{sc}) and/or large V_{oc}, the devices exhibit relatively modest FF. Indeed, even good organic solar cells exhibit considerably lower FFs ~0.7 than the best perovskite 0.8-0.85 and inorganic devices, ~0.87.[2] In particular, most of these high efficiency organic devices have active layers around 100 nm only. Increasing the thickness is beneficial for enhancing the light absorption and, favourable for high-throughput solution processing techniques at lower cost and less defect density.[3] However, when the active layer thickness is increased, the FF and, with that, the overall PCE are reduced significantly for the majority of polymer/fullerene or non-fullerene combinations. Reduced FF can be imagined as the manifestation of voltage dependent charge photogeneration and inefficient free

charge extraction in competition with non-geminate recombination.[4,5] Several reports have indicated that the geminate recombination of initially generated charge pairs at the donor/acceptor interface can be a significant loss pathway limiting the photocurrent generation, in particular, for those with highly intermixed donor−acceptor blends.[6–8] In other disordered systems, various reports showed that photocurrent at short circuit current is limited by non-geminate recombination.[9–11] However, there are significant variations in the literature over the factors limiting the FF of organic photovoltaics (OPV) devices including selectivity of the contacts.[12,13]

Recently a novel Naphtho[1,2-c:5,6-c′]Bis([1,2,5]Thiadiazole)-based polymer (NT812) has been introduced with power conversion efficiencies as high as 10% in junctions with thickness of several hundreds of nm – very exceptional results for OSCs.[14] In previous work we presented charge transport and recombination properties of NT812:PCBM[70] and found significantly suppressed bimolecular recombination in this system.[15] In this study, we employ both steady state and transient electro-optical measurements to disentangle geminate and non-geminate loss processes in NT812 when blended with PCBM[70] and ITIC devices (see **scheme 1** and **Figure S1** for chemical structure and energy levels). We investigate possible reasons for the lower FF in ITIC blends.

Indeed, a detailed study of charge carrier generation, recombination, and extraction reveals different properties for these two acceptor systems. Our results indicate that despite a 0.2 eV smaller LUMO-LUMO offset in the NT812:ITIC blend and the lower electron mobility, this system still generates as efficient photocurrent as NT812:PCBM[70] device, at short circuit current. However the photocurrent in ITIC blend degrades more with approaching V_{OC} in NT812:ITIC resulting in a lower FF compared to NT812:PCBM[70]. Whilst both systems exhibits

field independent charge generation, the NT812:ITIC device unveils more non-geminate recombination.

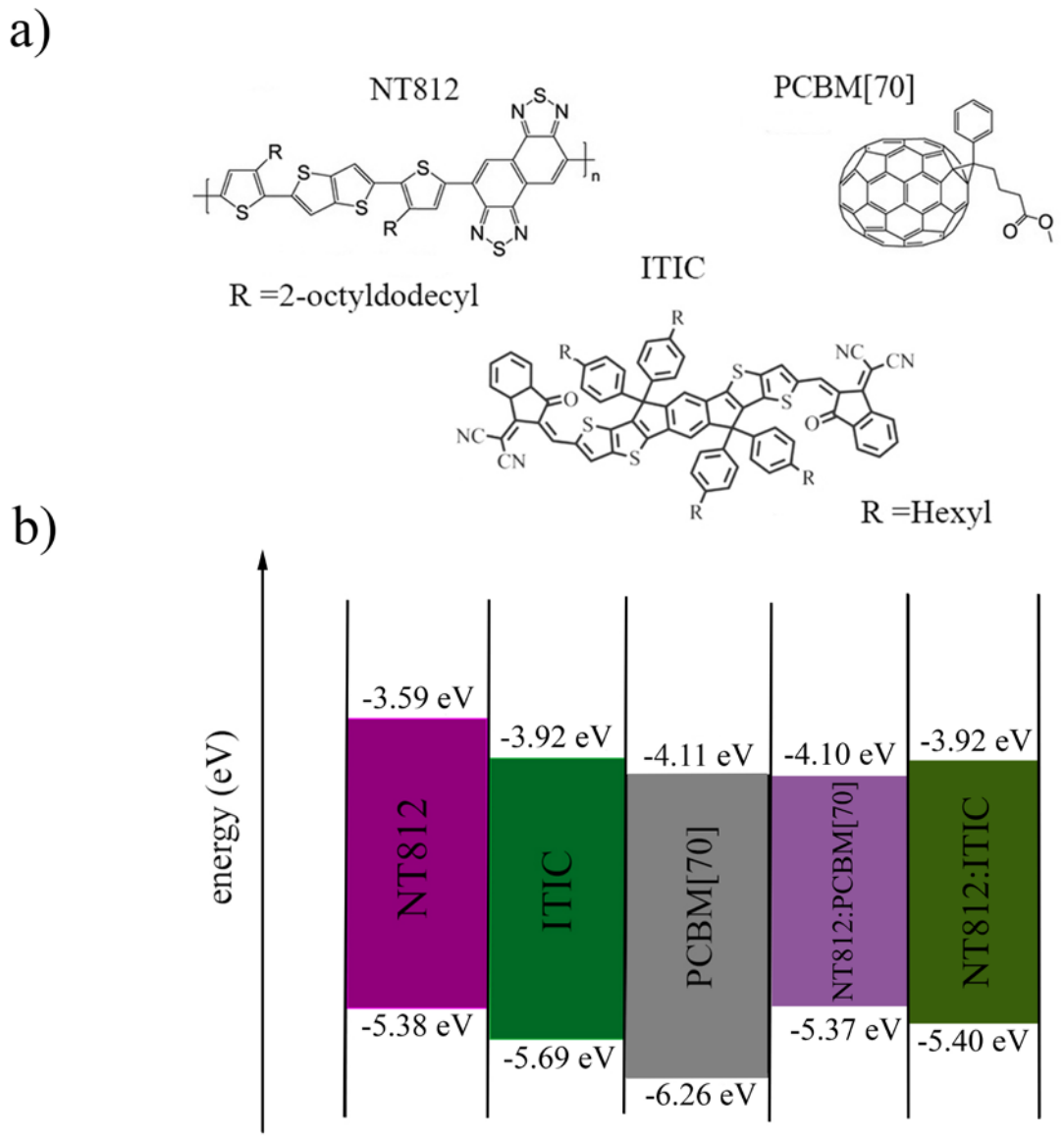

Scheme 1. a) Chemical structure of NT812, ITIC and PCBM[70], b) Photochemical energy level diagram for neat and blend films, obtained from CV measurements, see **Figure S1**.

2. Results and discussion

Figure 1 shows current–voltage (*JV*) curves for 100 nm thick BHJ solar cells under simulated 1 sun illumination. The NT812:PCBM[70] device exhibits 8.0% PCE with an V_{OC} of 0.76 V, a J_{SC} of 14.3 mAcm^{-2} and a FF of 73%. The NT812:ITIC device exhibits a slightly higher J_{SC} and V_{OC} of 16.2 mAcm^{-2} and 0.81 V respectively, however a lower FF of 55%, which reduces the efficiency to 7.3%. Whilst the PCEs in 100 nm thick junction devices are not too different, the ITIC device exhibits a non-negligible gradient at short circuit, indicating that the observed J_{SC} and FF are reduced by loss mechanisms already effective at short circuit. As photon absorption is voltage-independent, this slope must be related to field dependent charge generation, or recombination/extraction.[16-18] We note that due to the small equilibrium charge carrier density in NT812:ITIC system any role of screening of built-in field due to the doping is negligible.[15] The smaller energy offsets in ITIC blend may be the cause of the slightly reduced exciton dissociation in this system (see **Figure S2** for photoluminescence quenching data (PLQ)), however based on literature on other systems[19] the data still suggests efficient dissociation of the exciton at the NT812:ITIC interface within the amorphous regions whilst pure polymer and or ITIC domains also co-exists (hence the lower PLQ). In the following, the differences in geminate and non-geminate recombination dynamics are presented in order to investigate the origin of the dramatic change in the FF.

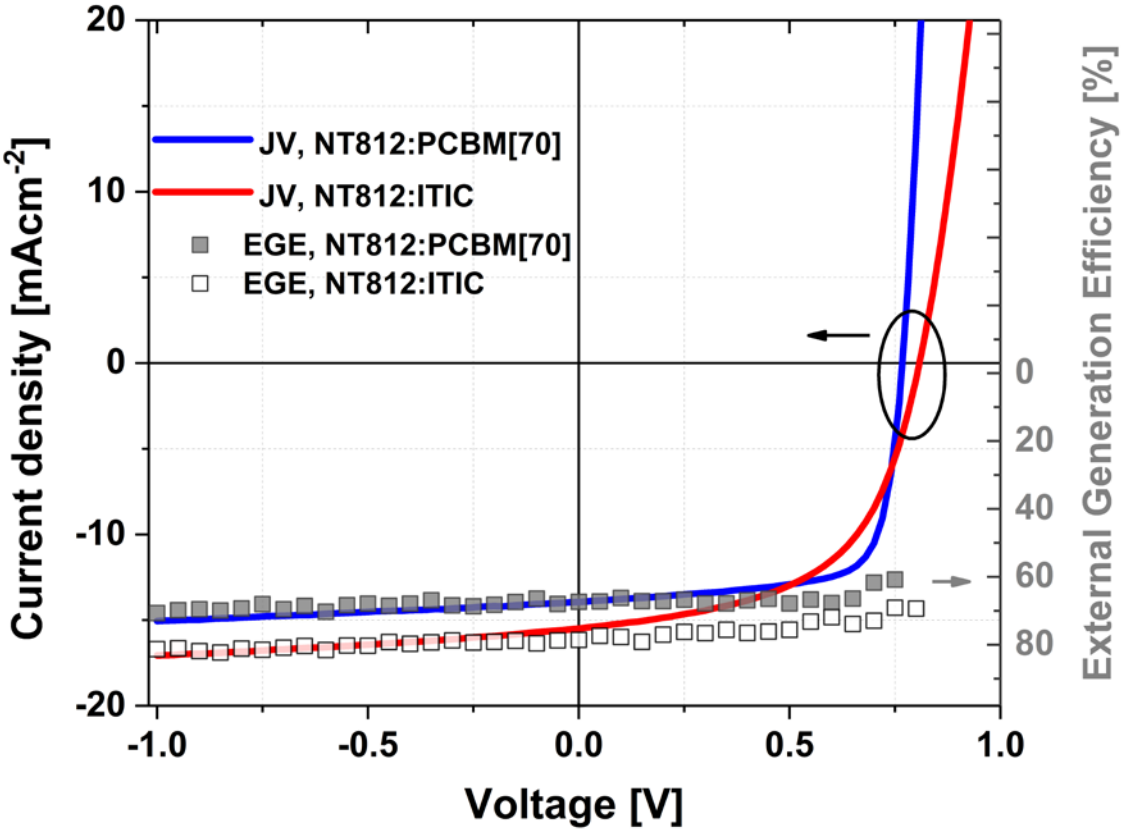

Figure 1. The external generation efficiency (EGE) which is mainly representative of geminate recombination for NT812:PCBM[70] and NT812:ITIC, measured with TDCF, as a function of pre-bias for 4ns delay time and fluences of ~0.02 μJ cm^{-2} at excitation wavelength of 532 nm with a laser pulse length of 6 ns. For comparison, the current density versus voltage (JV) characteristics of the same device under simulated AM 1.5 G light calibrated to 100 mW cm^{-2} is shown by a solid line.

Charge transport properties

To investigate charge transport properties of BHJ solar cells, electron and hole mobilities (μ_e and μ_h) and equilibrium charge carrier concentration need to be quantified. We performed resistance

dependent photovoltage (RPV) and space charge limited current (SCLC) measurements (see **Figure S3**) to determine the carrier mobilities.[20]

RPV setup is similar to time-of-flight, where charge carriers are photogenerated by a short low intensity laser pulse (such that the electric field inside the device is undisturbed. Unique to the RPV, the entire measurement is repeated at many different load resistances. The transient photosignal is determined by the competition between the transport of charge carriers inside the film, and the response of the external RC circuit. Typical data is shown in **Figure S3**; results are tabulated in **Table 1**.

In the ITIC system, using RPV we determine balanced carrier mobilities of ~1.4×10^{-4} cm^2 V^{-1} s^{-1}. This balanced mobility is confirmed through the SCLC measurements where the electron and hole mobilities are extracted to be 4.5×10^{-4} and 3.7×10^{-4} cm^2 V^{-1} s^{-1}, respectively. The electron mobility in the blend with ITIC is about an order of magnitude lower than typical PCBM[70] electron mobility in efficient blends with sufficient fullerene loading.[21,22] We had previously measured hole and electron mobilities of 4×10^{-4} and 2×10^{-3} cm^2 V^{-1} s^{-1} respectively, in NT812:PCBM[70] devices.[15]

There are differing views on the importance of mobility balance from the theoretical perspective; most simulations have predicted photogeneration to suffer strongly from imbalanced mobilities.[23] In addition, the preferential extraction of only one carrier type is well-known to cause space charge of the slower species to build up.[22,24] The creation of space charge suppresses the overall charge carrier collection efficiency due to the screening of the built-in electric field – this is especially the case in the thick junction but has been argued to play a detrimental role in thin solar cells (~100 nm).[22] In this regard, it is anticipated that the ITIC blend takes advantage of its balanced mobilities.

However, it is a general consensus that low mobilities are detrimental to charge generation and extraction,[21] which in part may be the cause of the lower FF in ITIC devices.

Table 1. electron and hole mobilities of NT812:ITIC device based on two type of measurements, SCLC and RPV.

Measurement	Electron mobility ($\boldsymbol{cm^2\ V^{-1}\ s^{-1}}$)	Hole mobility ($\boldsymbol{cm^2\ V^{-1}\ s^{-1}}$)
SCLC	4.5×10^{-4}	3.7×10^{-4}
RPV	1.4×10^{-4}	1.4×10^{-4}

Charge generation

To understand the poorer FF in NT812:ITIC blends, charge generation and recombination were studied in detail with a combination of different steady-state and transient methods. A poor FF may originate from a field dependent dissociation of CT states into free carriers, and /or significant bimolecular recombination of the free carriers. The former is mostly dependent on the driving force to dissociate CT states to free charges and the latter is a typical characteristic of low mobility disordered systems.

We employed time-delayed collection field (TDCF) measurements to elucidate on the nature of charge generation and recombination as described in previous work.[25] In TDCF measurements, the device is held at a particular pre-bias while excitons are photogenerated with a laser pulse. At that certain bias, any geminate and non-geminate recombination may occur, and after a specified delay time, a reverse bias is applied to collect all extractable charges that have survived geminate and non-geminate recombination. When these experiments are conducted under very low fluences

and at short delay times, non-geminate recombination is minimized during charge carrier extraction and thus the total extracted charge per photons absorbed is representative of the external generation efficiency (EGE). The EGE can be obtained as a function of voltage. At longer delay times and higher fluences, TDCF can yield information about non-geminate recombination of free carriers.

Figure 1 shows the JV curves of NT812:ITIC and NT812:PCBM[70] devices along with the EGE as a function of voltage (total charge plotted versus the pre-bias voltage at a delay time, t_d=4 ns at very low fluence (~0.02 μJcm^{-2}). The *JV* curves are well described by our EGE at V < 0.25 V for NT812:PCBM[70] and V < 0 V for NT812:ITIC. This means that the device photocurrent is generated exactly with the charges measured by TDCF at short delay times. It is also evident that in PCBM[70] devices there is no effect of pre-bias on generation, while the ITIC exhibits about 3% loss from -1 V to J_{SC}, which is insignificant; previous reports have demonstrated systems with much higher field dependent charge generation.[26]

This finding suggests that free charge photogeneration in both ITIC and PCBM[70] systems proceeds in a fashion where there is a low barrier for charge transfer state dissociation into free carriers. This may be either due to entropy,[27] and / or high local mobility.[28]

In ITIC and PCBM[70] blends, based on high photoluminescence quenching yields and high photocurrent densities, we anticipate the co-existence of both mixed and pure domains, whereby an energetic sink is established that drives and stabilizes the photogenerated charges out of the intermixed regions.[19] The rather weak or even absent field dependence of generation seen in ITIC and PCBM[70] is consistent with this structural picture.

Non-geminate recombination

Non-geminate recombination occurs as free charges travel through the film and encounter the opposite charge at the interface between donor and acceptor bulk heterojunction to form a CT state. This CT state may decay to the ground state and effectively an electron and a hole are recombined non-geminately to the ground state. The simplest description of charge carrier recombination is Langevin's model in which encounter rate is consider as $k_L = q(\mu_h + \mu_e)/\varepsilon_r\varepsilon_0$ where q is elementary charge; ε_r and ε_0 are relative and vacuum permittivity, respectively; μ_e and μ_h are electron and hole mobilities. In this model, the encounter rate of electrons and holes is determined with the sum of electron and hole mobilities. A more realistic modification of the encounter rate, k_{en} which is relevant to BHJ systems with nano-domains has been presented by Heiber et al.[29] given by **Equation 1.**

$$k_{\mathrm{en}} = \left(\mu_h^g + \mu_e^g\right)^{\frac{1}{g}} f(d)\ \frac{q}{\varepsilon_r\varepsilon_0} \equiv \gamma_{\mathrm{geo}} k_L \qquad (1)$$

where g is a domain size dependent power mean exponent and *f*(*d*) a morphological reduction prefactor due to the confinement of the carrier in their respective domains. γ_{geo} is the overall geometrical reduction factor of bimolecular recombination relative to the Langevin rate (sum of mobilities) explained in previous works.[30] However, often many systems typically show a significant departure from this type of recombination. As such the recombination of free carriers can be expressed by the rate equation

$$R = k_{\mathrm{rec}} n^2 = \gamma k_L n^2 \qquad (2)$$

$$\gamma = \gamma_{\mathrm{CT}} \times \gamma_{\mathrm{geo}} \qquad (3)$$

where k_{rec} is the recombination coefficient for bimolecular recombination, γ the overall bimolecular recombination reduction factor relative to Langevin rate (k_L) and γ_{CT} the reduction

factor due to the efficient recycling the CT states in some systems (see below). Therefore, γ has to have two major components. γ_{geo} is the reduction factor due to the reduced encounter rate of charges at the interface, with respect to the Langevin rate. Heiber et al. have found that this reduction factor is not significant for domain sizes relevant to efficient solar cells.[29] The other component that reduces the recombination, γ_{CT}, is related to the kinetics of the charge transfer states. When the dissociation rate of the free carriers is much faster than the decay rate of the singlet CT states to the ground and back electron transfer rate of the triplet CT states to triplet excitons, this effectively results in suppressed recombination rate of free charges to the ground state.[31]

We employed steady state bias assisted charge extraction (BACE) to probe the nature of recombination.[32] In BACE measurements, the device under steady state illumination is held at the pre-bias voltage which is exactly the VOC at the given illumination intensity. Under this condition, the recombination of free carriers is equal to the charge generation (G) so that

$$R = G = \frac{J_{sat}}{q.d} \qquad (4)$$

where J_{sat} and d are the saturated current at reverse bias voltage and the thickness of the device, respectively. When the LED is turned off, the external bias is rapidly changed to the reverse bias in order to extract all carriers; hence, the recombination coefficient for bimolecular recombination (k_{rec}) is determined.

Our measurements indicate that k_{rec} measured for ITIC blend is 8×10^{-17} m^3 s^{-1} at 1 sun, with dependence on charge-carrier density, as shown in **Figure 2**.

This recombination coefficient is rather high and it is only 5 times less than its Langevin recombination coefficient (k_L) for this system as shown by the dash line. NT812:PCBM[70] however exhibit much smaller k_{rec}, yielding 43 times reduced recombination than its Langevin recombination limit. In the SI we present a comparison between the measured data with that of the literature, on the competition factor between charge extraction and second-order bimolecular recombination as defined by Bartesaghi et al.[4] (see **Figure S4**). Previous report has suggested 800 times reduced recombination for NT812:PCBM[70],[15] however we note that NT812 has a different molecular weight in this study and also yields lower efficiency compared to the previous work.

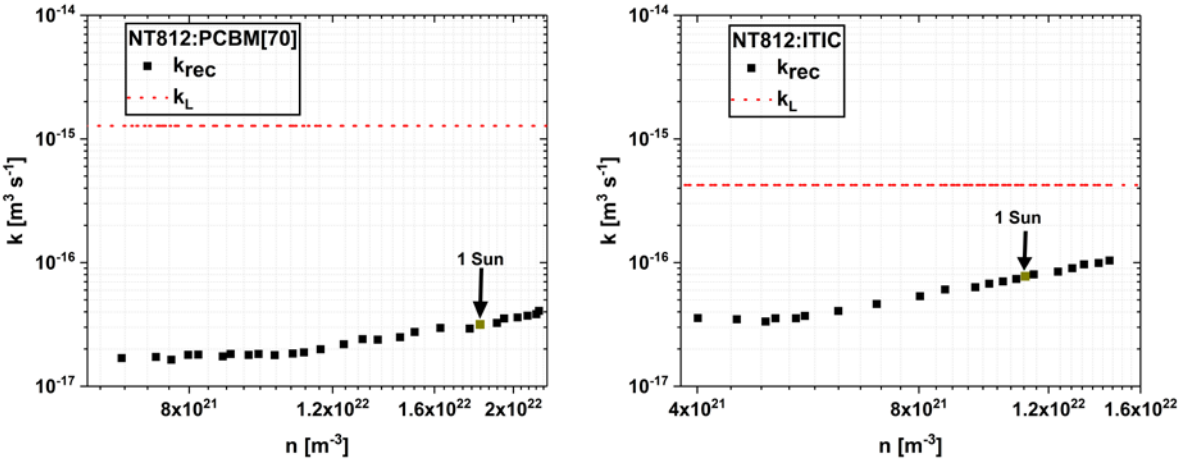

Figure 2. Bimolecular recombination coefficient as a function of carrier intensity, obtained from BACE measurement (solid squares) and Langevin recombination (dash line) for NT812:PCBM[70] and NT812:ITIC.

Concerning charge recombination, from pre-bias dependent TDCF measurements at different delay times between excitation and extraction, we observe that whilst both devices exhibit a dependence of extraction on pre-bias, the PCBM device however, shows an almost invariant behaviour with the delay time, whilst the ITIC system shows a strong dependence of extracted

carriers on the delay time. One can see that in the range of -1 V to V_{OC}, in the ITIC system almost 50% of charges have survived from recombination at 200 ns compared to 80% at 20 ns. In PCBM however, 80% of charges survive recombination at 200 ns, compared to 85% at 20 ns. Of particular interest is that in the PCBM system, loss in extraction due to the delay time, independent of fluence, only occurs at around 50 mV below its V_{OC}, whilst the ITIC system shows loss of extraction from an early pre-bias of -0.5 V. These results illustrate important findings. First, a slightly stronger field dependence is present in the ITIC system. Secondly, this field dependence of the extracted charges is strongly dependent on the delay time in NT812:ITIC device, suggesting a fast non-geminate recombination. In the PCBM system, however, the recombination is strikingly very slow and almost invariant in time. Consequently, the TDCF results at a delay of 4 ns suggest that in fact, whilst generation of free charge carriers occurs equally efficient up to J_{SC} for both systems (**Figure 1**) the rate of recombination of these photogenerated charges differs significantly (**Figure 3**). The importance of these findings are reflected when considering the superposition principle. Superposition principle is often used to describe the total *JV* characteristics of solar cells in which the current flowing in illuminated devices at a bias voltage *V* is the shift of a voltage-independent saturated photocurrent and the dark current – explained by the Shockley diode equation. The *JV* curve of the NT812:ITIC device under illumination cannot to be reconstructed from the dark *JV* as shown in **Figure 4**, and reflects the invalidity of the superposition approximation for this (and most organic semiconductor) systems when the photocurrent is assumed voltage independent. NT812:PCBM on the other hand, shows that the shifted dark current does reproduce the *JV* curve under illumination reasonably well.

a)

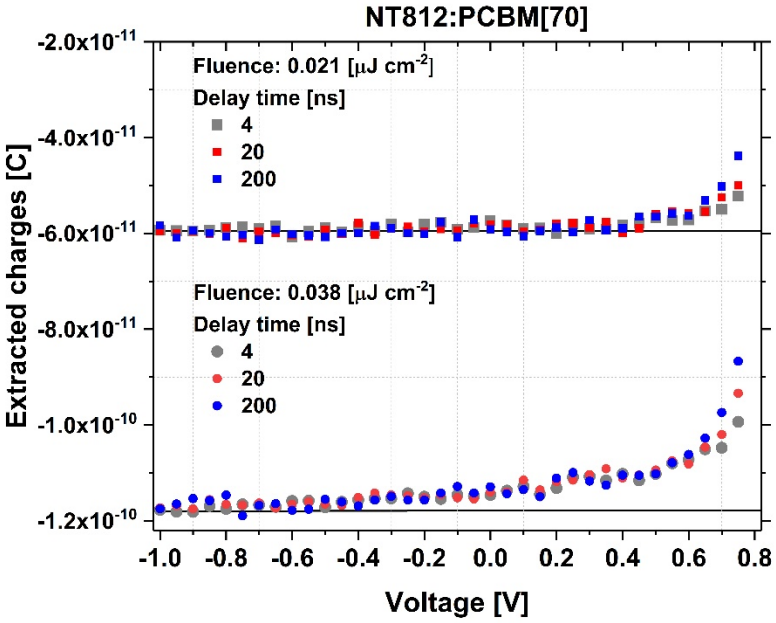

b)

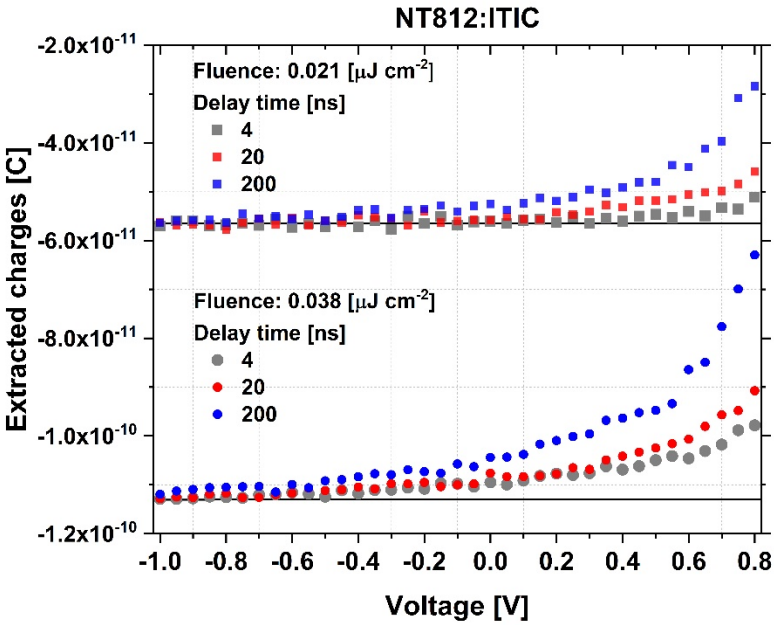

Figure 3. Extracted charges versus pre-bias voltage at different delay times between the pre-bias and the collection voltage for a) NT812:PCBM[70] and b) NT812:ITIC devices at two laser intensities.

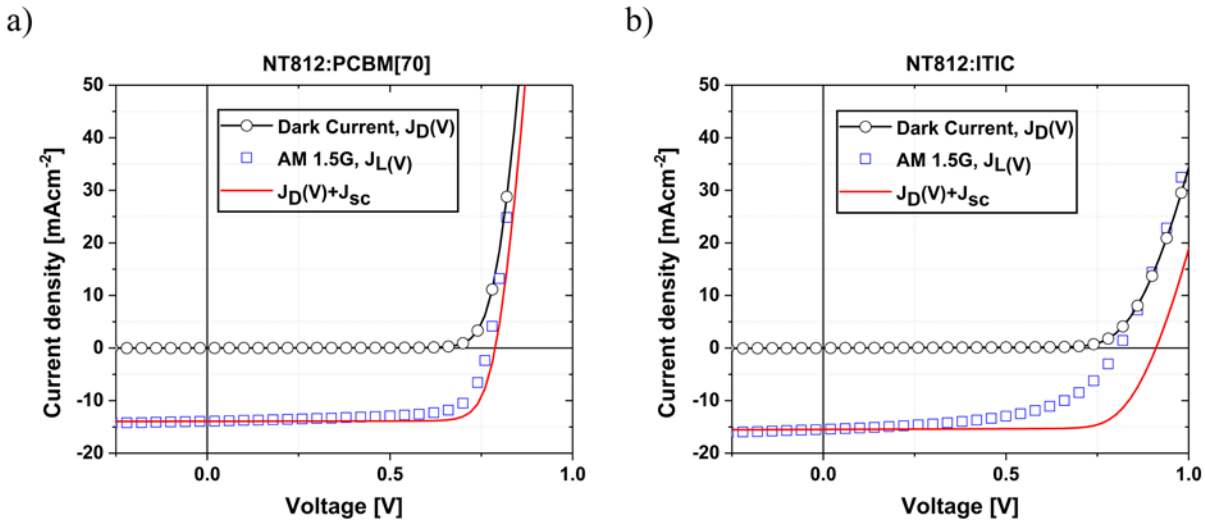

Figure 4. JV characteristics of a) NT812:PCBM[70] and b) NT812:ITIC under simulated AM 1.5G light calibrated to 100mW cm^{-2}. The circle with black line and blue squares shows dark and light current, respectively. Shifted dark by J_{sc} is shown with red solid line.

The study herein addresses the factors determining the fill factor of blend devices employing NT812 with ITIC and with PCBM[70]. Overall, we find that the variation in FF between these two acceptors is not primarily determined by variations in light absorption, nor by variations in exciton separation efficiency. Rather this variation is determined by differences in charge recombination affecting charge collection efficiency.

Among the many studies of organic solar cells employing NFAs, most studies have focused rather on the importance of exciton separation and/or carrier mobility in limiting photocurrent generation. However, the consideration of CT state losses, with respect to Langevin recombination in limiting bimolecular recombination has been completely absent from the NFA literature to date.

In **Figure 5** we have plotted the predicted diffusion limited reduction factors (γ_{geo}) for different domain sizes based on the model of Heiber et al.[29] [Equation (1)] versus the square root of the

mobilities product assuming an electron mobility of 1.4 x 10^{-4} cm^2 V^{-1} s^{-1}. Plotting the measured reduction factor (γ) of the NT812:ITIC and NT812:PCBM[70] system on the same figure demonstrates that the ITIC reduction factor is only five times larger than the predicted encountered recombination whilst PCBM[70]'s reduction factor significantly departs from the model, regardless of the domain size or the nano-morphology. This implies that the origin of the fast recombination in the ITIC system and the non-Langevin recombination in the PCBM[70] device is predominantly controlled by the kinetics of the CT state.

This raises the question of the importance of the charge transfer state (CTS). All recombination occurs through CT states. Whilst encounter limited recombination is indeed relevant for forming the intermediate CTS, the final loss mechanism is, however, limited by the back electron transfer of ^{3}CT to triplet excitons or geminate recombination of the ^{1}CT state to the ground state.[33] In NT812:PCBM[70], the suppressed recombination is assigned to the slower loss decay and back electron transfer rate of the CT states compared to their dissociation rate which results in equilibrium between the CTS and free charges.[15] We note that the this kinetic completion is very sensitive to the active layer's morphology and even for the same material system, one can observe different kinetics by changing the processing conditions or the molecular weight of the polymer. In contrast, in case of the ITIC system, the recombination rate is mostly encounter limited.

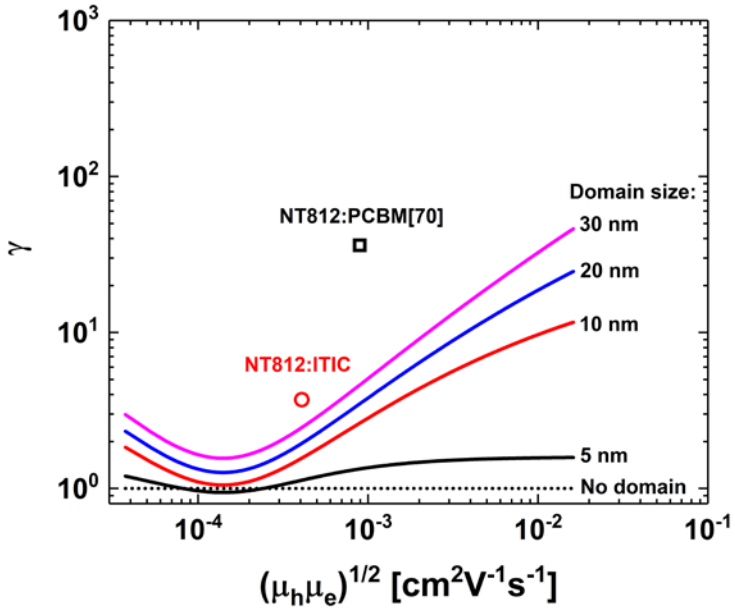

Figure 5. Predicted diffusion controlled reduction factors of the bimolecular recombination for different domain sizes (coloured lines, calculated based on Heiber et al.[29]) as a function of the square root of the mobilities assuming an electron mobility of 1.4 x 10^{-4} cm^2 V^{-1} s^{-1}, compared the measured reduction factor for NT812:ITIC and NT812:PCBM[70].

It is of interest that despite the smaller energy offsets and moderately lower photoluminescence quenching of the excitons in the ITIC system, the loss in CTS generation does not translate into a loss in EGE or photocurrent; rather similar EGE and photocurrent at J_{SC} are generated in this blend compared to the PCBM[70] blend. This is consistent with previous studies on comparison of charge generation between fullerene and non-fullerene blends, where it has been concluded that NFA blends show as efficient (if not better) charge generation.[34–37] However, in contrast to previously reported NFA, perylene diimides systems in particular, the increased non-geminate recombination in ITIC is not assigned to spatially trapped charge carriers in isolated domains, rather to faster recombination of the free carriers.

Experimental section

Solar-Cell Fabrication and Characterization: Patterned indium tin oxide (ITO)-glass substrates were pre-cleaned successively with detergent, acetone, de-ionized (DI) water and IPA and dried by nitrogen. The dried substrates were treated by oxygen plasma at room temperature for 4 min and then coated with PEDOT:PSS by spin-coating (3000 r.p.m. for 30 s, thickness of ≈40 nm) and were then baked at 150 °C for 15 min in air. For deposition of active layers, blend solution of polymer (NT812 with polydispersity index, PDI≈ 2) and PCBM[70] at a weight ratio of 1:1.5 dissolved in CB:DCB = 3:1 (with 0.5 vol% of 1-chloronaphthalene) and blend solution of polymer:ITIC at a weight ratio of 1.3:1, based on optimum device efficiency (see Table S1 for different blend ratio), dissolved in o-xylene (with 1 vol% of 1-Methyl-2-pyrrolidinone) were spin-cast on top of the PEDOT:PSS layer in a nitrogen-filled glove box. The active-layer thickness was controlled by changing the concentration of the solution; typically an active layer of 100 nm thickness can be achieved by 4 and 9 mg mL^{-1} solution (based on polymer concentration) for NT812:PCBM[70] and NT812:ITIC, respectively. Thermal annealing of the blend films was carried out by placing them on a hot plate at 100 °C for 15 min and 160 °C for 20 min for NT812:PCBM[70] and NT812:ITIC, respectively, in a nitrogen atmosphere. A 5 nm PFN-Br layer was then spin-coated from methanol solution onto the active layers. The thin films were transferred into a vacuum evaporator connected to the glove box, and Ag (100 nm) was deposited sequentially through a shadow mask under $\approx 1 \times 10^{-7}$ mbar, with an active area of the cells of A = 0.011 cm^2 for BACE and TDCF measurement, and A = 0.06 cm^2 for JV measurement.

UV-Visible absorption and Photoluminescence (PL) spectroscopy: UV-Visible spectra of the thin films were acquired with Cary 5000 UV-Vis-NIR spectrophotometer in air. The PL spectra were measured with a Fluorolog-3 spectrofluorometer (Horiba Jobin Yvon). All film samples were spin coated on glass substrates.

Time Delayed Collection Field: In the TDCF experiment, a laser pulse from a diode pumped, Q-switched Nd:YAG laser (NT242, EKSPLA) with 6 ns pulse duration and a typical repetition rate of 500 Hz working at 532 nm were used to generate charges in the device. A pulse generator (Agilent 81150A) was used to apply the pre- and collection bias which are amplified by a home-built amplifier. The current through the device was measured via a grounded 10 Ω resistor in series with the sample and with a differential current probe recorded with an oscilloscope (DSO9104H). The pulse generator was triggered with a fast photodiode (EOT, ET-2030TTL). The fluence was determined with a CCD-camera in combination with a calibrated photodiode sensor (Ophir) and a laser-cut high-precision shadow mask to define the illuminated area.

Bias Assisted Charge Extraction: The experimental setup required for BACE measurements was similar to the TDCF setup, except for the illumination conditions. The steady state condition was established by a high power 1 W, 638 nm laser diode (insaneware) with a switch off time of about 10 ns. The LED was operated at 500 Hz with a duty cycle of at least 50% of one period, which means 1ms of illumination before the diode was switched off for 1 ms. After switching off the laser diode, a high reverse bias was applied and all charges were extracted. The fast switch off time of the diode and the fast pulse generator (Agilent 81150A) allowed for charge extraction as

fast as 10–20 ns after the switch off. The current transients were measured via a grounded 10 Ω resistor and recorded with an oscilloscope (DSO9104H) in the same way as for the TDCF measurement.

Resistance dependent Photo Voltage: Photocurrent and photovoltage transients were recorded using a digital storage oscilloscope (DSO9104H) via a LabVIEW code. A pulsed second-harmonic Nd:YAG laser (NT242, EKSPLA) working at 450 nm was used with 6 ns pulse duration. The laser beam with ~50 mJ energy output was attenuated with a natural optical-density (OD) filter set. Low laser pulse fluences (~OD 7) were used for the RPV mobility measurements in order to prevent a redistribution (screening) of the internal electric field and maintaining quasi-short-circuit conditions regardless of the load resistance.

3. Conclusion

In summary, we compare device performance between ITIC and PCBM when blended with NT812 polymer. The ITIC system demonstrates a blend with balance carrier mobilities, and a high V_{OC} and J_{SC} whilst exhibiting a FF that is affected by field dependent mechanisms. We show that the field dependence limiting the FF stems from fast time-dependent non-geminate recombination. On the other hand, the PCBM system exhibits strikingly slow non-geminate recombination and reduced recombination. Slowing down the non-geminate recombination, to shift the balance towards non-Langevin systems, is important for both improving the power conversion efficiency and also for achieving thick junction devices.

ASSOCIATED CONTENT

Supporting Information

The Supporting Information on photochemical energy level, photoluminescence quenching, mobility measurements, figure of merit and device performance of NT812:ITIC are available free of charge on the ACS Publications website.

AUTHOR INFORMATION

Corresponding Author

*E-mail: shoai@uni-potsdam.de

Funding Sources

Authors declare no competing financial interest.

ACKNOWLEDGMENT

This work was funded by Alexander von Humboldt Foundation (Sofja Kovalevskaja award), the German Ministry of Science and Education (BMBF) within the project UNVEIL, FKZ 13N13719 and the Deutsche Forschungsgesellschaft (DFG) Projekt Nr. NE 410/13-1, NE410/15-1, INST 336/94-1 FUGG.

REFERENCES

(1) Zhang, G.; Zhao, J.; Chow, P. C. Y.; Jiang, K.; Zhang, J.; Zhu, Z.; Zhang, J.; Huang, F.; Yan, H. Nonfullerene Acceptor Molecules for Bulk Heterojunction Organic Solar Cells. *Chem. Rev.* **2018**, *118*, 3447–3507.

(2) Green, M. A.; Emery, K.; Hishikawa, Y.; Warta, W. Solar Cell Efficiency Tables (Version 37). *Prog. photovoltaics Res. Appl.* **2011**, *19*, 84–92.

(3) Meredith, P.; Armin, A. LED Technology Breaks Performance Barrier. *Nature* **2018**, *562*, 197–198.

(4) Bartesaghi, D.; del Carmen Pérez, I.; Kniepert, J.; Roland, S.; Turbiez, M.; Neher, D.; Koster, L. J. A. Competition between Recombination and Extraction of Free Charges Determines the Fill Factor of Organic Solar Cells. *Nat. Commun.* **2015**, *6*, 7083.

(5) Heiber, M. C.; Okubo, T.; Ko, S.-J.; Luginbuhl, B. R.; Ran, N.; Wang, M.; Wang, H.; Uddin, M. A.; Woo, H. Y.; Bazan, G. C. Measuring the Competition between Bimolecular Charge Recombination and Charge Transport in Organic Solar Cells under Operating Conditions. *Energy Environ. Sci.* **2018**, *11*, 3019-3032

(6) Marsh, R. A.; Hodgkiss, J. M.; Friend, R. H. Direct Measurement of Electric Field-Assisted Charge Separation in Polymer: Fullerene Photovoltaic Diodes. *Adv. Mater.* **2010**, *22*, 3672–3676.

(7) Albrecht, S.; Schindler, W.; Kurpiers, J.; Kniepert, J.; Blakesley, J. C.; Dumsch, I.; Allard, S.; Fostiropoulos, K.; Scherf, U.; Neher, D. On the Field Dependence of Free Charge Carrier Generation and Recombination in Blends of PCPDTBT/PC 70BM: Influence of Solvent Additives. *J. Phys. Chem. Lett.* **2012**, *3*, 640–645.

(8) Mingebach, M.; Walter, S.; Dyakonov, V.; Deibel, C. Direct and Charge Transfer State Mediated Photogeneration in Polymer–fullerene Bulk Heterojunction Solar Cells. *Appl. Phys. Lett.* **2012**, *100*, 106.

(9) Wetzelaer, G. A. H.; Van der Kaap, N. J.; Koster, L. J. A.; Blom, P. W. M. Quantifying Bimolecular Recombination in Organic Solar Cells in Steady State. *Adv. Energy Mater.* **2013**, *3*, 1130–1134.

(10) Guo, J.; Ohkita, H.; Benten, H.; Ito, S. Charge Generation and Recombination Dynamics in Poly (3-Hexylthiophene)/Fullerene Blend Films with Different Regioregularities and Morphologies. J. Am. *Chem. Soc.* **2010**, *132*, 6154–6164.

(11) Rauh, D.; Deibel, C.; Dyakonov, V. Charge Density Dependent Nongeminate Recombination in Organic Bulk Heterojunction Solar Cells. *Adv. Funct. Mater.* **2012**, *22*, 3371–3377.

(12) Wheeler, S.; Deledalle, F.; Tokmoldin, N.; Kirchartz, T.; Nelson, J.; Durrant, J. R. Influence of Surface Recombination on Charge-Carrier Kinetics in Organic Bulk Heterojunction Solar Cells with Nickel Oxide Interlayers. *Phys. Rev. Appl.* **2015**, *4*, 24020.

(13) Sandberg, O. J.; Nyman, M.; Dahlström, S.; Sandén, S.; Smått, J.-H.; Österbacka, R. Quantifying Loss-Mechanisms Related to Charge Carrier Collection in Thin-Film Solar Cells, *Proceedings of SPIE*, San Diego, California, United States, Sept 18, **2018**; *10737*, 107370A.

(14) Jin, Y.; Chen, Z.; Dong, S.; Zheng, N.; Ying, L.; Jiang, X. F.; Liu, F.; Huang, F.; Cao, Y. A Novel Naphtho[1,2-c:5,6-C′]Bis([1,2,5]Thiadiazole)-Based Narrow-Bandgap π-Conjugated Polymer with Power Conversion Efficiency Over 10%. *Adv. Mater.* **2016**, *28*, 9811–9818.

(15) Armin, A.; Chen, Z.; Jin, Y.; Zhang, K.; Huang, F.; Shoaee, S. A Shockley-Type Polymer: Fullerene Solar Cell. *Adv. Energy Mater.* **2018**, *8*, 1701450.

(16) Kirchartz, T.; Agostinelli, T.; Campoy-Quiles, M.; Gong, W.; Nelson, J. Understanding the Thickness-Dependent Performance of Organic Bulk Heterojunction Solar Cells: The Influence of Mobility, Lifetime, and Space Charge. *J. Phys. Chem. Lett.* **2012**, *3*, 3470–3475.

(17) Koster, L. J. A.; Smits, E. C. P.; Mihailetchi, V. D.; Blom, P. W. M. Device Model for the Operation of Polymer/Fullerene Bulk Heterojunction Solar Cells. *Phys. Rev. B* **2005**, *72*, 085205.

(18) Mauer, R.; Howard, I. A.; Laquai, F. Effect of Nongeminate Recombination on Fill Factor in Polythiophene/ Methanofullerene Organic Solar Cells. *J. Phys. Chem. Lett.* **2010**, *1*, 3500–3505.

(19) Shoaee, S.; Subramaniyan, S.; Xin, H.; Keiderling, C.; Tuladhar, P. S.; Jamieson, F.; Jenekhe, S. A.; Durrant, J. R. Charge Photogeneration for a Series of Thiazolo-Thiazole Donor Polymers Blended with the Fullerene Electron Acceptors PCBM and ICBA. *Adv. Funct. Mater.* **2013**, *23*, 3286–3298.

(20) Philippa, B.; Stolterfoht, M.; Burn, P. L.; Juška, G.; Meredith, P.; White, R. D.; Pivrikas, A. The Impact of Hot Charge Carrier Mobility on Photocurrent Losses in Polymer-Based Solar Cells. *Sci. Rep.* **2014**, *4*, 5695.

(21) Stolterfoht, M.; Armin, A.; Shoaee, S.; Kassal, I.; Burn, P.; Meredith, P. Slower Carriers Limit Charge Generation in Organic Semiconductor Light-Harvesting Systems. *Nat. Commun.* **2016**, *7*, 11944.

(22) Armin, A.; Juska, G.; Ullah, M.; Velusamy, M.; Burn, P. L.; Meredith, P.; Pivrikas, A. Balanced Carrier Mobilities: Not a Necessary Condition for High-Efficiency Thin Organic Solar Cells as Determined by MIS-CELIV. *Adv. Energy Mater.* **2014**, *4*, 1300954.

(23) Athanasopoulos, S.; Tscheuschner, S.; Bässler, H.; Köhler, A. Efficient Charge Separation of Cold Charge-Transfer States in Organic Solar Cells through Incoherent Hopping. *J. Phys. Chem. Lett.* **2017**, *8*, 2093–2098.

(24) Mihailetchi, V. D.; Wildeman, J.; Blom, P. W. M. Space-Charge Limited Photocurrent. *Phys. Rev. Lett.* **2005**, *94*, 126602.

(25) Kniepert, J.; Schubert, M.; Blakesley, J. C.; Neher, D. Photogeneration and Recombination in P3HT/PCBM Solar Cells Probed by Time-Delayed Collection Field Experiments. *J. Phys. Chem. Lett.* **2011**, *2*, 700–705.

(26) Kurpiers, J.; Ferron, T.; Roland, S.; Jakoby, M.; Thiede, T.; Jaiser, F.; Albrecht, S.; Janietz, S.; Collins, B. A.; Howard, I. A. Probing the Pathways of Free Charge Generation in Organic Bulk Heterojunction Solar Cells. *Nat. Commun.* **2018**, *9*, 2038.

(27) Hood, S. N.; Kassal, I. Entropy and Disorder Enable Charge Separation in Organic Solar Cells. *J. Phys. Chem. Lett.* **2016**, *7*, 4495–4500.

(28) Shoaee, S.; Stolterfoht, M.; Neher, D. The Role of Mobility on Charge Generation, Recombination, and Extraction in Polymer-Based Solar Cells. *Adv. Energy Mater.* **2018**, 1703355.

(29) Heiber, M. C.; Baumbach, C.; Dyakonov, V.; Deibel, C. Encounter-Limited Charge-Carrier Recombination in Phase-Separated Organic Semiconductor Blends. *Phys. Rev. Lett.* **2015**, *114*, 136602.

(30) Armin, A.; Subbiah, J.; Stolterfoht, M.; Shoaee, S.; Xiao, Z.; Lu, S.; Jones, D. J.; Meredith, P. Reduced Recombination in High Efficiency Molecular Nematic Liquid Crystalline: Fullerene Solar Cells. *Adv. Energy Mater.* **2016**, *6*, 1600939.

(31) Armin, A.; Durrant, J. R.; Shoaee, S. Interplay between Triplet-, Singlet-Charge Transfer States and Free Charge Carriers Defining Bimolecular Recombination Rate Constant of Organic Solar Cells. *J. Phys. Chem. C* **2017**, *121*, 13969–13976.

(32) Kniepert, J.; Lange, I.; Van Der Kaap, N. J.; Koster, L. J. A.; Neher, D. A Conclusive View on Charge Generation, Recombination, and Extraction in As-Prepared and Annealed P3HT: PCBM Blends: Combined Experimental and Simulation Work. *Adv. Energy Mater.* **2014**, *4*, 1301401.

(33) Ferguson, A. J.; Kopidakis, N.; Shaheen, S. E.; Rumbles, G. Dark Carriers, Trapping, and Activation Control of Carrier Recombination in Neat P3HT and P3HT: PCBM Blends. *J. Phys. Chem. C* **2011**, *115*, 23134–23148.

(34) Shoaee, S.; Deledalle, F.; Tuladhar, P. S.; Shivanna, R.; Rajaram, S.; Narayan, K. S.; Durrant, J. R. A Comparison of Charge Separation Dynamics in Organic Blend Films Employing Fullerene and Perylene Diimide Electron Acceptors. *J. Phys. Chem. Lett.* **2015**, *6*, 201–205.

(35) Shoaee, S.; Clarke, T. M.; Huang, C.; Barlow, S.; Marder, S. R.; Heeney, M.; McCulloch, I.; Durrant, J. R. Acceptor Energy Level Control of Charge Photogeneration in Organic Donor/Acceptor Blends. *J. Am. Chem. Soc.* **2010**, *132*, 12919–12926.

(36) Song, X.; Gasparini, N.; Ye, L.; Yao, H.; Hou, J.; Ade, H.; Baran, D. Controlling Blend Morphology for Ultrahigh Current Density in Nonfullerene Acceptor-Based Organic Solar Cells. *ACS Energy Lett.* **2018**, *3*, 669–676.

(37) Wadsworth, A.; Ashraf, R. S.; Abdelsamie, M.; Pont, S.; Little, M.; Moser, M.; Hamid, Z.; Neophytou, M.; Zhang, W.; Amassian, A. Highly Efficient and Reproducible Nonfullerene Solar Cells from Hydrocarbon Solvents. *ACS Energy Lett.* **2017**, *2*, 1494–1500.

a)

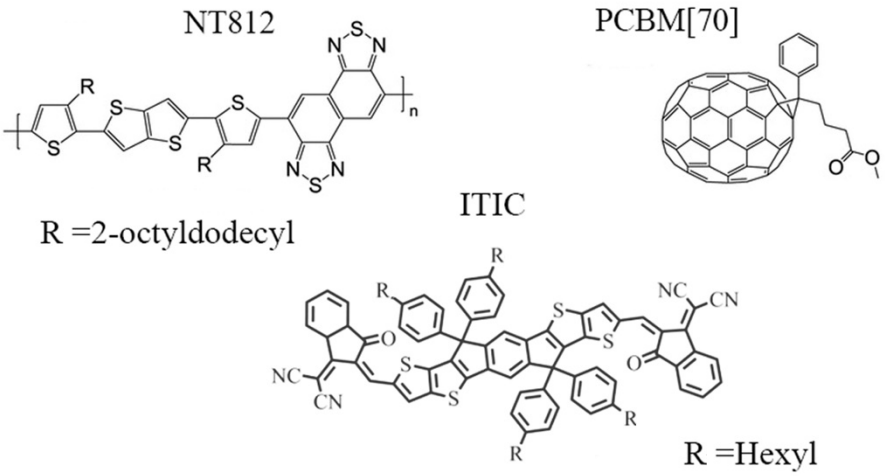

b)

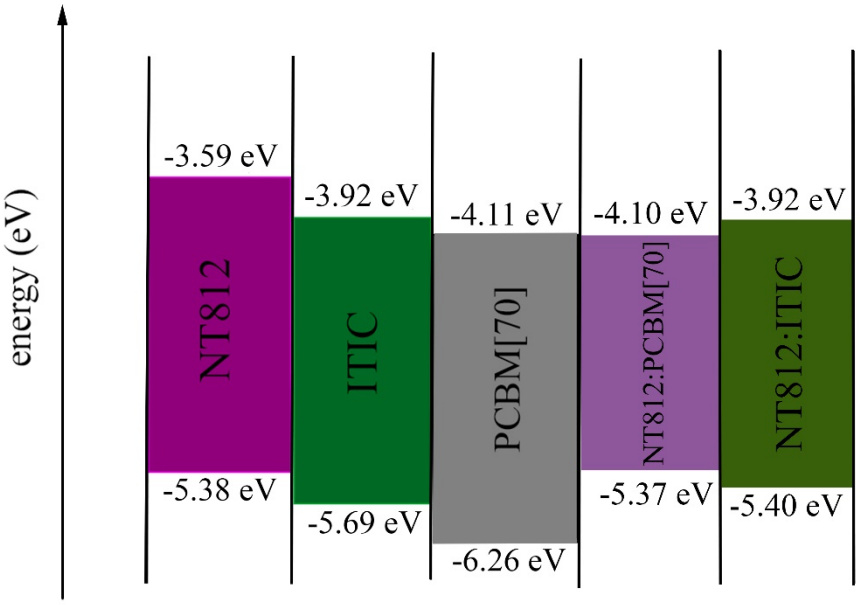

Scheme 1. a) Chemical structure of NT812, ITIC and PCBM[70], b) Photochemical energy level diagram for neat and blend films, obtained from CV measurements, see **Figure S1**.

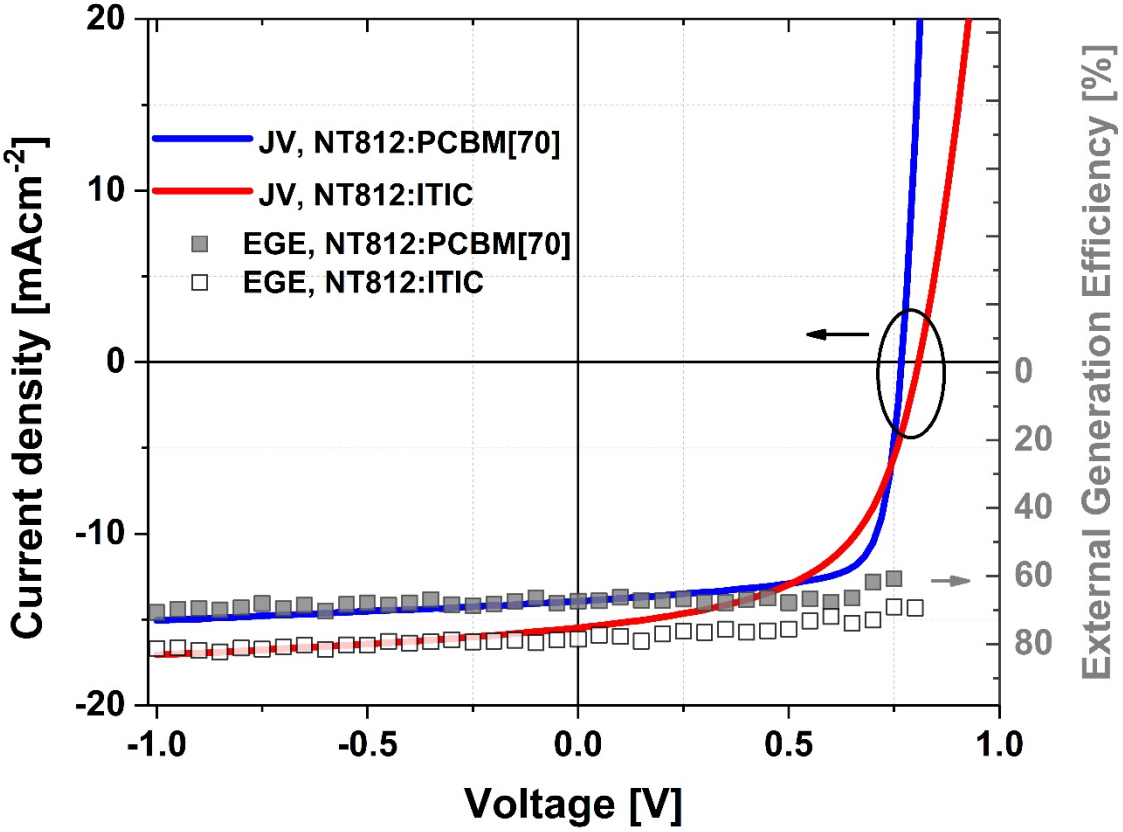

Figure 1. The external generation efficiency (EGE) of NT812:PCBM[70] and NT812:ITIC, measured with TDCF, as a function of pre-bias for 4ns delay time and fluences of ~0.02 μJ cm^{-2} at excitation wavelength of 532 nm with a laser pulse length of 6 ns. For comparison, the current density versus voltage (JV) characteristics of the same device under simulated AM 1.5 G light calibrated to 100 mW cm^{-2} is shown by a solid line.

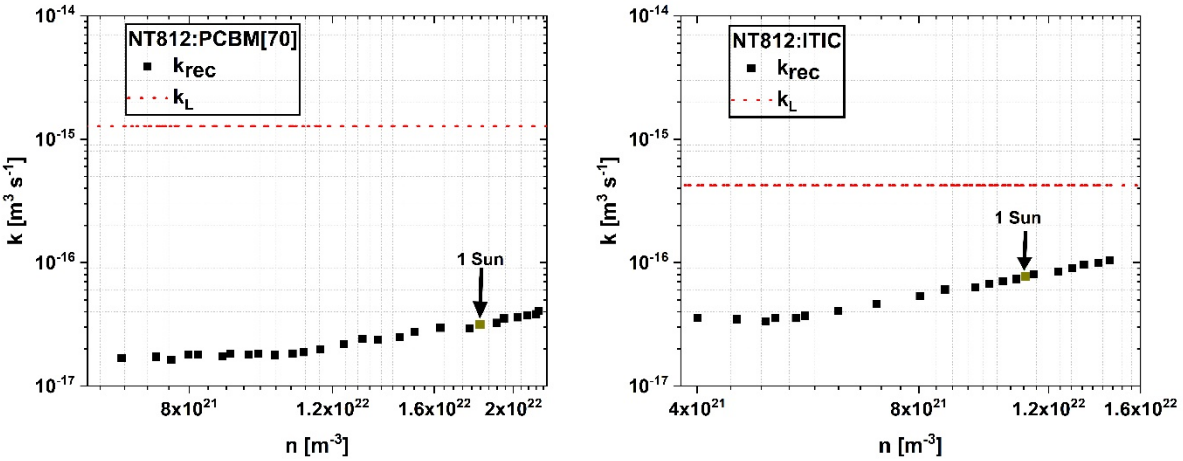

Figure 2. Bimolecular recombination coefficient as a function of carrier intensity, obtained from BACE measurement (solid squares) and Langevin recombination (dash line) for NT812:PCBM[70] and NT812:ITIC.

a)

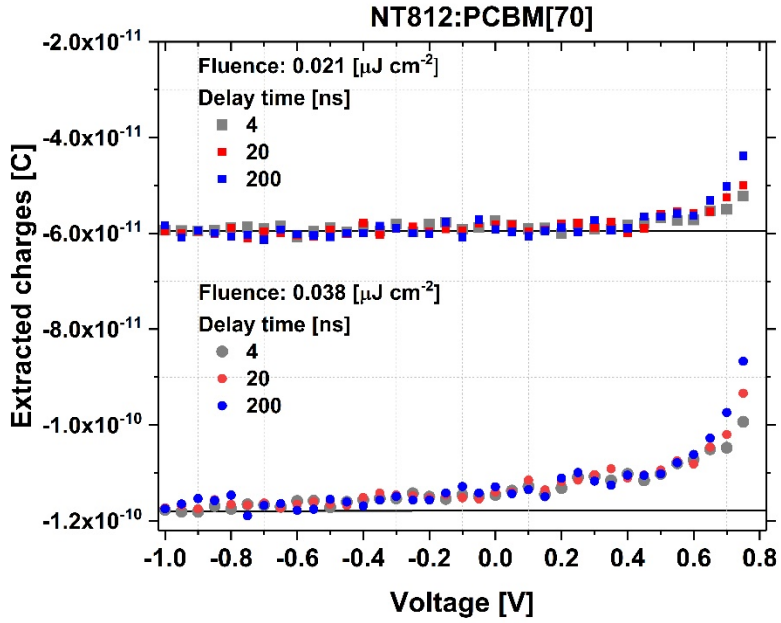

b)

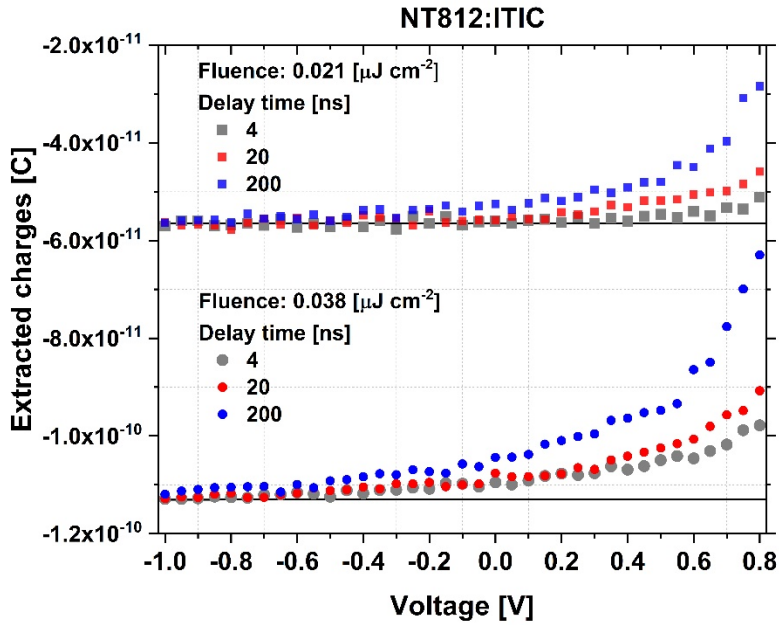

Figure 3. Extracted charges versus pre-bias voltage at different delay times between the pre-bias and the collection voltage for a) NT812:PCBM[70] and b) NT812:ITIC devices at two laser intensities.

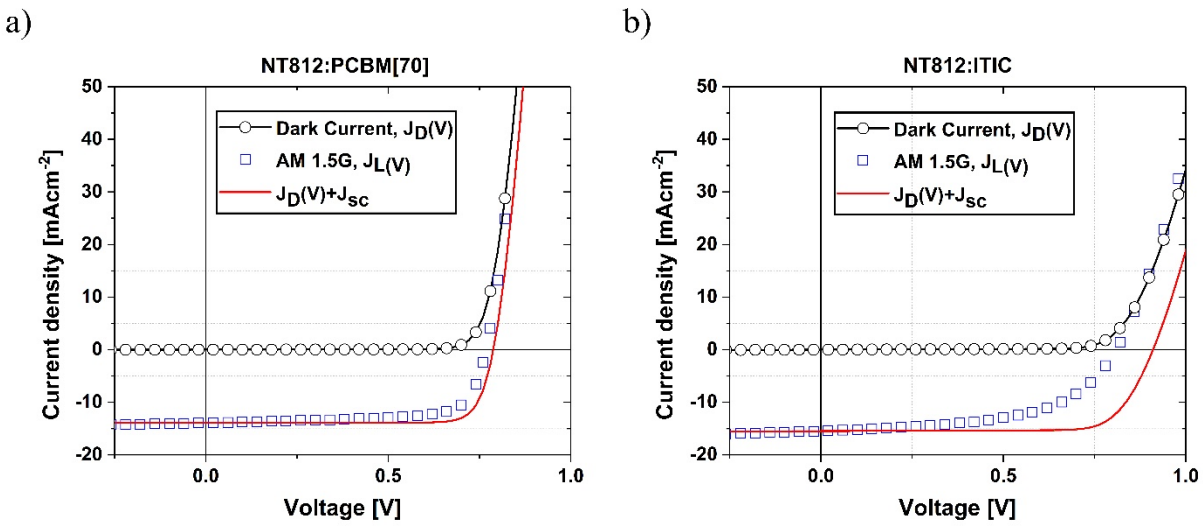

Figure 4. JV characteristics of a) NT812:PCBM[70] and b) NT812:ITIC under simulated AM 1.5G light calibrated to 100mW cm^{-2}. The circle with black line and blue squares shows dark and light current, respectively. Shifted dark by J_{sc} is shown with red solid line.

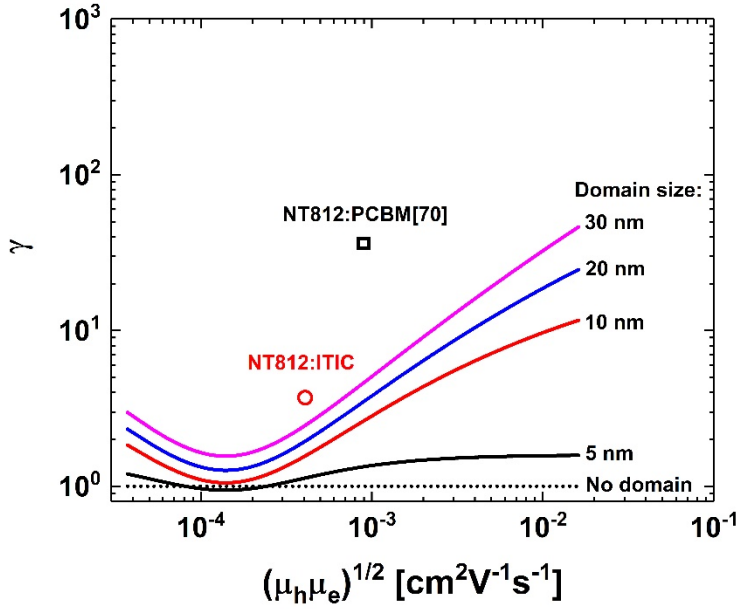

Figure 5. Predicted diffusion controlled reduction factors of the bimolecular recombination for different domain sizes (coloured lines, calculated based on Heiber et al.[29]) as a function of the square root of the mobilities assuming an electron mobility of 1.4 x 10^{-4} cm^2 V^{-1} s^{-1}, compared the measured reduction factor for NT812:ITIC and NT812:PCBM[70].

Table 1. electron and hole mobilities of NT812:ITIC device based on two type of measurements, SCLC and RPV.

Measurement	Electron mobility ($\boldsymbol{cm^2\ V^{-1}\ s^{-1}}$)	Hole mobility ($\boldsymbol{cm^2\ V^{-1}\ s^{-1}}$)
SCLC	4.5×10^{-4}	3.7×10^{-4}
RPV	1.4×10^{-4}	1.4×10^{-4}

TOC Graphic

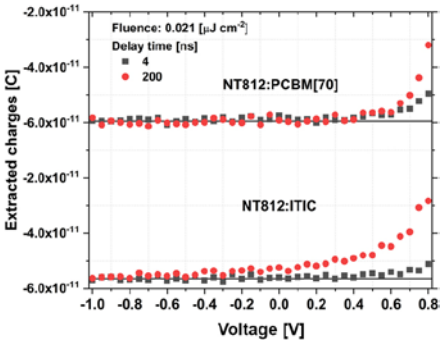
Fluence: 0.021 [μJ cm-2]
Delay time [ns]
4
200
NT812:PCBM[70]
NT812:ITIC
Extracted charges [C]
Voltage [V]
-2.0x10-11
-4.0x10-11
-6.0x10-11
-2.0x10-11
-4.0x10-11
-6.0x10-11
-1.0
-0.8
-0.6
-0.4
-0.2
0.0
0.2
0.4
0.6
0.8